

# Optimal Design of Multi-Layer Fog Collectors

Musaddaq Azeem,<sup>†</sup> Adrien Guérin,<sup>‡,⊥</sup> Thomas Dumais,<sup>‡</sup> Luis Caminos,<sup>‡</sup> Raymond E. Goldstein,<sup>¶</sup> Adriana I. Pesci,<sup>¶</sup> Juan de Dios Rivera,<sup>§</sup> María Josefina Torres,<sup>||</sup> Jakub Wiener,<sup>†</sup> José Luis Campos,<sup>‡</sup> and Jacques Dumais<sup>\*,‡</sup>

<sup>†</sup>*Technical University of Liberec, Faculty of Textile Engineering, Department of Material Engineering, Studentská 1402/2, 461 17, Liberec 1, Czech Republic*

<sup>‡</sup>*Universidad Adolfo Ibáñez, Faculty of Engineering and Sciences, Av. Padre Hurtado 750, Viña del Mar, Chile*

<sup>¶</sup>*University of Cambridge, Department of Applied Mathematics and Theoretical Physics, Cambridge, UK*

<sup>§</sup>*Pontificia Universidad Católica de Chile, Departamento de Ingeniería Mecánica y Metalúrgica, Santiago, Chile*

<sup>||</sup>*Pontificia Universidad Católica de Valparaíso, Escuela de Ingeniería Mecánica, Av. Los Carrera, Quilpué, Chile*

<sup>⊥</sup>*Current address: Université Paris 7 Diderot, Laboratoire Matière et Systèmes Complexes, Paris, France*

E-mail: jacques.dumais@uai.cl

Phone: +56 32 2503712

## Abstract

The growing concerns over desertification have spurred research into technologies aimed at acquiring water from non-traditional sources such as dew, fog, and water vapor. Some of the most promising developments have focused on improving designs to collect water from fog. However, the absence of a shared framework to predict, measure and compare the water collection efficiencies of new prototypes is becoming a major obstacle to progress in the field. We address this problem by providing a general theory to design efficient fog collectors as well as a concrete experimental protocol to supply our theory with the parameters necessary to quantify the effective water collection efficiency. We show in particular that multi-layer collectors are required for high fog collection efficiency and that all efficient designs are found within a narrow range of mesh porosity. We support our conclusions with measurements on simple multi-layer harp collectors.

## Keywords

fluid mechanics, fog collector, harp design, porous media, water collection efficiency

# 1 Introduction

Many regions of the world experience chronic water shortages and the associated impacts on human health and economic growth.<sup>1</sup> This crisis has spurred research for novel technologies to exploit alternative water sources such as fog,<sup>2,3</sup> dew,<sup>4-6</sup> and even water vapor.<sup>7</sup> Where the conditions are favorable, fog stands out as one of the most attractive water sources because fog water can, in principle, be collected in large amounts without any input of energy.<sup>8-10</sup> Accordingly, a large body of work has focused on the design of efficient fog collectors.<sup>11-18</sup> Fog collection is usually achieved with fine meshes exposed to the incoming fog stream. The minuscule fog droplets intercepted by the threads accumulate until they reach a critical size at which point the force of gravity overcomes the surface tension forces and allow the drop to slide down the collector's surface to reach the gutter at its base.

The central design challenge for efficient fog collection must reconcile two physical processes that have opposite requirements.<sup>19</sup> On the one hand, fog collecting meshes cannot be very dense or present a major obstacle to the flow of air otherwise the incoming fog stream will simply bypass the structure laterally. On the other hand, fog droplets can be intercepted only if they encounter a mesh element while they transit through the collector. Therefore, overly open meshes are poor collectors, just as meshes that are too dense. A related issue for fog collectors is clogging of the mesh by the water droplets that have been captured thus making the collector less permeable to the incoming fog and reducing the overall water collection efficiency.<sup>11</sup> Material scientists have sought to alleviate the problem of clogging by making structural changes to the mesh such as using harp designs<sup>17,20</sup> or branched patterns<sup>21,22</sup> instead of using the standard criss-crossing meshes that tend to trap water drops. Other material science contributions have explored modifications of the collecting surfaces to allow intercepted droplets to coalesce and move quickly under the action of gravity.<sup>23-25</sup> In particular, modifications of the contact angle hysteresis can reduce the critical size a drop needs to reach before it is freed from the mesh.<sup>11</sup> Unfortunately, many of these possible improvements will have to be scaled to realistic sizes ( $>1 \text{ m}^2$ ) and produced at a competitive

28 price (less than \$25USD per m<sup>2</sup>)<sup>26</sup> before they can be implemented in the field.

29 An alternative avenue to improve the performance of fog collectors arises from observa-  
30 tions of the bromeliad *Tillandsia landbeckii*, a plant that relies almost exclusively on fog to  
31 fulfill its water needs. *Tillandsia* forms large stands on the fog-prone coast of the Atacama  
32 Desert of Chile. These stands are striking in that the plants self-organize into bands orthog-  
33 onal to the flow of fog (Fig. 1A), thus allowing each plant direct access to the fog stream.  
34 Moreover, the leaves and stems of *Tillandsia* are reduced to thin filamentous structures orga-  
35 nized into a three-dimensional mesh, a unique feature among bromeliads (Fig. 1B). Finally, a  
36 dense layer of hydrophilic trichomes covers the plant surfaces (Fig. 1C). Three length scales  
37 emerge from observations of *Tillandsia*: the smallest length scale is that of the trichomes  
38 ( $\sim 100 \mu\text{m}$ ) involved in intercepting fog droplets, the intermediate length scale is the char-  
39 acteristic pore size between the leaves ( $\sim 1 \text{ mm}$ ) through which the fog stream must filter,  
40 the largest length scale is the self-organization of *Tillandsia* plants into fog collecting stands  
41 ( $\geq 1 \text{ m}$ ). These observations indicate that 3-D structures, with appropriately selected length  
42 scales, can be efficient at collecting fog.

43 Inspired by *Tillandsia landbeckii*, we investigated the potential offered by multi-layer  
44 designs for improving the water collection efficiency of fog collectors (Fig. 1D). Such 3-D  
45 structures can resolve many of the issues associated with single-layer collectors, including  
46 clogging. Despite having been field tested more than 50 years ago;<sup>27</sup> the performance multi-  
47 layer collectors has not been studied theoretically with the exception of one recent study.<sup>28</sup>  
48 Specifically, it is still unclear whether broadly applicable design principles exist. Here, we  
49 formalize the fundamental tradeoff associated with the capture of fog with multi-layer col-  
50 lectors and demonstrate that simple design rules can guarantee nearly optimal fog collection  
51 efficiency.

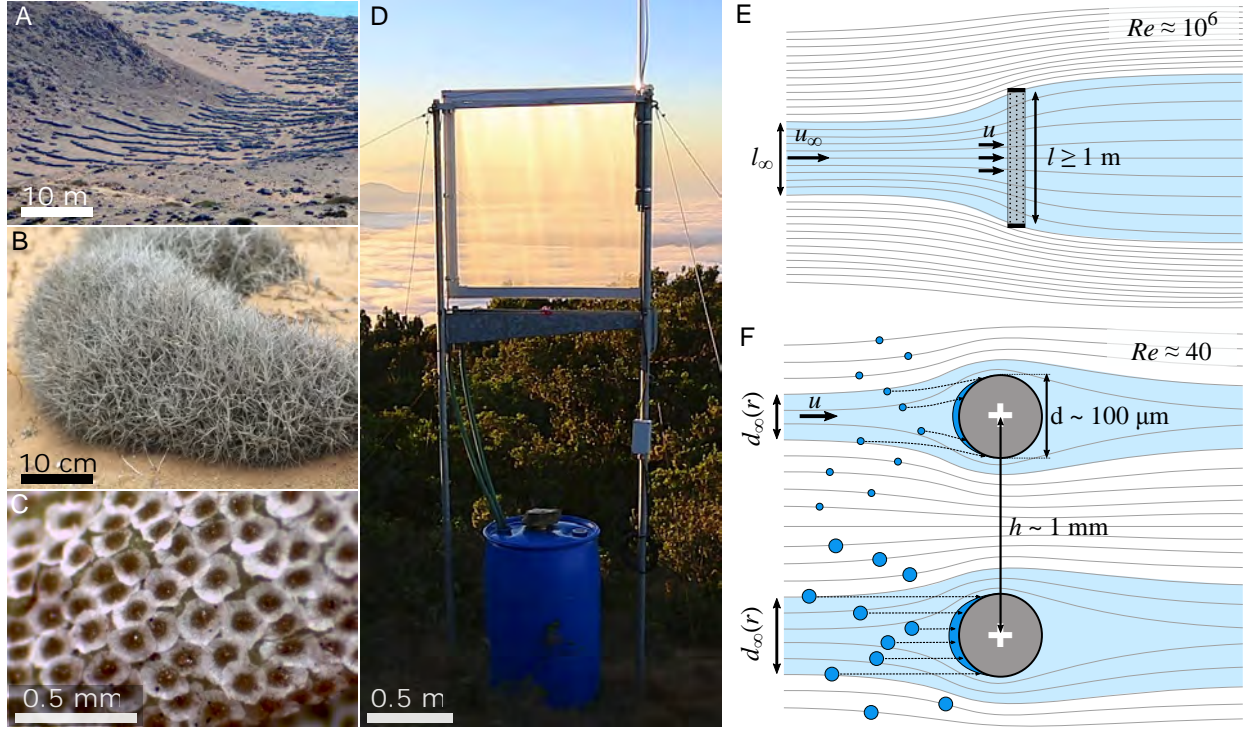


Figure 1: Aerodynamics of fog collection. (A) A stand of the bromeliad *Tillandsia landbeckii* in the Atacama Desert of Chile. (B) Close-up of *Tillandsia landbeckii* showing the dense three-dimensional array of leaves. (C) The hydrophilic scale-like trichomes covering the leaves and branches of *Tillandsia*. (D) Prototype of a  $1 \text{ m} \times 1 \text{ m}$  multi-layer fog collector with a mesh solidity  $s = 0.3$  per layer and  $N = 4$  layers. (E) Top view of the air flow around a fog collector. The typical collector length is  $1 \text{ m} \leq l \leq 10 \text{ m}$ . Streamlines are drawn based on wind tunnel experiments of Ito and Garry,<sup>29</sup> with a square mesh gauze of solidity 0.63 at  $Re = 10^5$  based on the collector size. (F) Close-up of the air flow around the section of two cylindrical threads of the collector. The diameter of the threads  $d \simeq 150 - 160 \mu\text{m}$  for the collector shown in (D) and the experiments discussed below.  $d_\infty(r)$  represents the span of streamlines whose droplets of radius  $r$  will be intercepted by the thread directly downstream. The top and bottom halves of the diagram show the interception of the small and large droplets, respectively; dashed lines indicate approximate trajectories of intercepted droplets. Streamlines are based on Goodman's simulations<sup>30</sup> at  $Re = 20$  based on the thread diameter.

## 2 Theory

### Total water collection efficiency $\eta_{tot}$

To formalize the performance of fog collectors, we define, as others have done before,<sup>19,28,31</sup> the total water collection efficiency ( $\eta_{tot}$ ) as the water flux coming out of the collector's gutter for each unit of collector area ( $J$ ,  $\text{g}\cdot\text{s}^{-1}\cdot\text{m}^{-2}$ ) divided by the liquid water flux of the unperturbed fog upstream of the collector:

$$\eta_{tot} = \frac{J}{LWC \cdot u_{\infty}}, \quad (1)$$

where  $LWC$  is the liquid water content of fog and  $u_{\infty}$  is the velocity of the unperturbed fog flow. A typical value for the  $LWC$  is  $0.5 \text{ g}\cdot\text{m}^{-3}$  while the characteristic fog velocity is  $3 - 5 \text{ m}\cdot\text{s}^{-1}$ .<sup>31,32</sup>

It is convenient to define  $\eta_{tot}$  in geometrical terms first by considering how a fog droplet upstream of the collector can ultimately be found in the flux of water  $J$  coming out of the collector's gutter. The initial stages of collection operate at different length scales (Figs. 1E,F). First, we consider what happens at the scale of the entire fog collector, where the characteristic Reynolds number is  $Re = ul/\nu \sim 10^6$  ( $\nu$  is the kinematic viscosity of air). Incoming fog droplets are part of an airstream that must filter through the collector if the droplets are to be captured. Since the collector is an obstacle to the free flow of the airstream, a fraction of the incoming fog will simply bypass the collector (Fig. 1E). The filtered fraction ( $\varphi$ ) can be quantified geometrically as the ratio of two areas:  $\varphi = A_{\infty}/A$ , where  $A_{\infty}$  is the area of the incoming fog flow that will filter through a collector of frontal area  $A$ . In the specific case of a square collector (Figs. 1D,E), the filtered fraction is  $\varphi = (l_{\infty}/l)^2$ .

The second collection stage takes place at a microscopic scale and pertains to the droplets transiting through the collector. Of these filtered droplets, only a subset will be on a trajectory that ensures collision with one of the collector elements (Fig. 1F). For any given

75 layer of the collector, the probability that a droplet collides with a thread is given by  $\frac{d_\infty(r)}{d}s$   
76 where the ratio  $d_\infty(r)/d$  represents the efficiency of inertial impaction for a droplet of radius  
77  $r$  (Fig. 1F) and  $s$  is the solid fraction, or solidity, of the layer ( $s = d/h$  for our harp design).  
78 Conversely, the probability that a droplet captured by a layer has a radius in the interval  
79  $[a, b]$  is  $s \int_a^b \frac{d_\infty(r)}{d} f(r) dr$ , where  $f(r)$  is the probability density function for fog droplet sizes.  
80 Given that the mass of water provided by a droplet scales with  $r^3$ , the relative contribution  
81 of droplets to the capture efficiency is  $\int_a^b \frac{d_\infty(r)}{d} m(r) dr$ , where

$$\int_a^b m(r) dr = \frac{\int_a^b r^3 f(r) dr}{\int_0^\infty r^3 f(r) dr} .$$

82  $\int_a^b m(r) dr$  is the mass fraction of liquid water contained in droplets with radii in the interval  
83  $[a, b]$ .<sup>33</sup>

84 Finally, to these two processes, we should add the drainage efficiency ( $\eta_{drain}$ ).<sup>19,28</sup> The  
85 drainage efficiency represents the fraction of the intercepted volume of water that ultimately  
86 reaches the tank of the collector. The drainage efficiency may be reduced by re-entrainment  
87 of captured droplets under high wind conditions<sup>27</sup> and potential leaks in the gutter and pipe  
88 leading to the collector's tank.

89 In the case of a single-layer collector, the three processes detailed above lead to the total  
90 water collection efficiency

$$\eta_{tot} = \eta_{ACE} \eta_{capt} \eta_{drain} = \underbrace{\left[ \frac{A_\infty s}{A} \right]}_{\eta_{ACE}} \underbrace{\left[ \int_0^\infty \frac{d_\infty(r)}{d} m(r) dr \right]}_{\eta_{capt}} \eta_{drain} , \quad (2)$$

91 where  $\eta_{ACE}$  is the Aerodynamic Collection Efficiency (ACE) introduced by Rivera.<sup>19</sup> When  
92 considering a collector with  $N$  layers, the total collection efficiency takes the form

$$\eta_{tot} = \frac{A_\infty}{A} \left[ 1 - \underbrace{\int_0^\infty \left( 1 - \frac{d_\infty(r)}{d} s \right)^N m(r) dr}_{\text{lost mass fraction}} \right] \eta_{drain} , \quad (3)$$

93 where the term  $\left(1 - \frac{d_{\infty}(r)}{d}s\right)^N$  is the probability that a drop of radius  $r$  traverses the  $N$   
94 layers of the collector without being intercepted (see also Demoz *et al.*<sup>34</sup>). Consequently,  
95 the integral represents the mass fraction of liquid water that filtered through the collector  
96 without being intercepted.

97 Three tacit assumptions were made to arrive at Eq. 3. These assumptions are listed  
98 here to define clearly the range of validity of our results. First, we assume that the incoming  
99 airflow both far-field and just upstream of the collector is orthogonal to the collector's surface.  
100 We justify this assumption because, as we shall see below, the optimum fog collectors are  
101 quite porous, with approximately 80% of the incoming fog flow passing through the collector.  
102 In this regime, the air velocity has a negligible component tangential to the collector surface  
103 (see Fig. 4E below), so the interaction of the airflow with the collector filaments does not  
104 depend on position within the collector. Second, we assume that  $\frac{d_{\infty}(r)}{d}$  is constant at all  
105 locations within the collector. This assumption implies a uniform mesh such as the harps  
106 under consideration but would have to be modified for meshes made of intersecting weft and  
107 warp threads and potentially differing in their size and shape. Third, in deriving the lost  
108 mass fraction, we make the hypothesis that the distance between the layers is sufficiently  
109 large to allow the fog stream to regain uniformity before reaching the next layer. As we will  
110 show below (Fig. 5A), the optimal inter-layer spacing ranges between 6 and 9 mm, which is  
111 at least 40 times greater than the characteristic thickness of the layers in our prototypes.

## 112 **Maximizing $\eta_{tot}$**

113 Because Eqs. 2 and 3 are geometrical definitions of  $\eta_{tot}$ , they are valid irrespective of the  
114 fluid mechanics model that might be developed to quantify the collection efficiency. Ideally,  
115 we would like to design the collector such that all steps in the harvesting of fog droplets  
116 are maximized to achieve a total water collection efficiency approaching unity. Our goal in  
117 this section is to demonstrate that  $\eta_{ACE}$  is the only component of  $\eta_{tot}$  that involves some  
118 fundamental design tradeoff.

119 We begin with the drainage efficiency,  $\eta_{drain}$  which is included in Eqs. 2 and 3 to take into  
 120 account the possibility that captured fog droplets are either re-entrained by the airstream  
 121 or otherwise lost due to leaks in the system. Although leaks need to be taken into account  
 122 in any implementation of a fog collector, they are outside the scope of a fluid mechanical  
 123 analysis. Re-entrainment needs to be considered more carefully. Two ways to eliminate it  
 124 are: (i) the use of multi-layer collectors to allow re-entrained drops to be re-captured by  
 125 a layer farther downstream<sup>27</sup> and (ii) the reduction in the size of the drops clinging to the  
 126 collector surface so that the drag on these drops does not exceed the critical value that would  
 127 cause them to detach. These design requirements are in fact among those put forward to  
 128 optimize the other aspects of the collection process, therefore the drainage efficiency will be  
 129 optimized *de facto*. In what follow, we set  $\eta_{drain} = 1$  and focus on the other terms of Eqs. 2  
 130 and 3.

131 At the operational *Re* number of fog collectors, the ratio  $d_{\infty}(r)/d$  reflects a deposition  
 132 mechanism by inertial impaction.<sup>20</sup> For a droplet of radius  $r$ , the efficiency of impaction  
 133 follows the relation<sup>20,35</sup>

$$\frac{d_{\infty}(r)}{d} = \frac{Stk}{Stk + \pi/2}, \quad (4)$$

134 where  $Stk = (2\rho_w r^2 u)/(9\mu d)$  is the Stokes number,  $\rho_w$  is the density of liquid water,  $u$  is  
 135 the velocity of the air stream,  $\mu$  is the dynamic viscosity of air, and  $d$  is the diameter of the  
 136 thread. This efficiency increases with increasing  $Stk$ ; however, we note from the definition  
 137 of  $Stk$  that the thread diameter  $d$  is the only parameter that can be tuned in the context  
 138 of a passive fog collector. Since  $Stk$  increases for decreasing  $d$ , the width of the elements  
 139 on which droplets are impacted should be reduced to a minimum. More precisely, Labbé  
 140 and coworkers<sup>20</sup> demonstrated that the size to be considered is the thread with the water  
 141 film or drops covering it. The reduction in the size of the collecting elements can be done  
 142 at constant solidity and without compromising other steps of the fog collection process.  
 143 Consequently, the geometrical ratio  $d_{\infty}(r)/d$  can be made as close to unity as one desires,  
 144 although maximizing  $d_{\infty}(r)/d$  for all droplet size classes is unwarranted since the smallest

145 droplets are the most challenging to capture and yet they represent a vanishingly small  
 146 fraction of the total *LWC* of fog.<sup>32</sup>

147 In what follows, we consider a small operating diameter for the collecting elements so  
 148 that  $d_\infty \rightarrow d$ . In this limit, Eq. 3 becomes:

$$\lim_{d_\infty \rightarrow d} \eta_{tot} = \eta_{ACE} = \underbrace{\frac{A_\infty}{A}}_\varphi \underbrace{[(1 - (1 - s)^N)]}_\chi \quad (5)$$

149 This equation captures in its most general form the Aerodynamic Collection Efficiency  
 150 ( $\eta_{ACE}$ ); that is, the fraction of droplets in an unperturbed upstream flow of area  $A$  that  
 151 are both filtered by ( $\varphi$ ), and incident to ( $\chi$ ), the elements of a multi-layer collector. The  
 152 ACE is of special significance because it encapsulates the fundamental trade-off in the design  
 153 of efficient fog collectors. While the incident fraction  $\chi$  increases with increasing solidity  $s$   
 154 and increasing number of layers  $N$ , the same parameter changes reduce the collector porosity  
 155 and therefore decrease the filtered fraction  $\varphi$ .

## 156 Fluid mechanical calculation of $A_\infty/A$

157 Determining ACE for a specific collector involves finding the ratio  $\varphi = A_\infty/A$  using the  
 158 design parameters of the collector, such as the solid fraction of the individual mesh layers  
 159 and the total number of layers. We first note that incompressibility of the flow together with  
 160 mass conservation imply  $Au = A_\infty u_\infty$  (Fig. 1E). Therefore, the geometrical definition of the  
 161 filtered fraction is also a statement about the ratio between the mean velocity across the  
 162 collector mesh and the velocity far upstream of the collector,

$$\varphi = \frac{A_\infty}{A} = \frac{u}{u_\infty} . \quad (6)$$

163 We follow the many earlier studies of fluid flow through and around porous structures  
 164 that equate two alternative definitions of the pressure drop across the porous material, the

165 first one at the scale of the porous medium and the second one at the scale of the far-field  
 166 flow. At the microscopic scale, the pressure drop is

$$\Delta P = k \frac{\rho_{air} u^2}{2}, \quad (7)$$

167 where  $\rho_{air}$  is the density of air and  $k$  is the pressure drop coefficient for the flow of an inviscid  
 168 fluid through a porous medium. This equation arises naturally from Bernoulli's principle.<sup>33</sup>  
 169 As we shall see, since  $k$  is typically not constant over a very large range of velocities, the  
 170 pressure drop coefficient is necessarily expressed in terms of the solid fraction of the medium  
 171 and the Reynolds number. At the scale of the entire collector, the pressure drop across the  
 172 mesh is also related to the drag coefficient  $C_D$ ,

$$\Delta P = \frac{F_D}{A} = C_D \frac{\rho_{air} u_\infty^2}{2}, \quad (8)$$

173 since the drag force  $F_D$  per unit area on the screen must equal the pressure drop. Eq. 8  
 174 represents the so-called “form drag” and is valid for blunt objects at high Reynolds numbers,  
 175 which is the case for fog collectors.<sup>36</sup> Equating the two pressure drops, we obtain the filtered  
 176 fraction

$$\varphi = \frac{A_\infty}{A} = \frac{u}{u_\infty} = \sqrt{\frac{C_D}{k}}. \quad (9)$$

177 This relation has been used in its various forms by Taylor,<sup>37</sup> Koo and James,<sup>38</sup> Steiros and  
 178 Hultmark<sup>39</sup> among many others.

179 There is no consensus on how to express the drag coefficient  $C_D$  and the pressure drop  
 180 coefficient  $k$  in terms of the design parameters of the collector mesh. To our knowledge, the  
 181 most recent and most complete treatment is due to Steiros and Hultmark<sup>39</sup> (later referred to  
 182 as Steiros2018); who extended the earlier work of Koo and James<sup>38</sup> by including the so-called  
 183 “base-suction” and thus obtained accurate predictions of the drag coefficient over the entire  
 184 range of solid fractions. According to their model, the drag and pressure drop coefficients

185 are

$$C_D = \frac{4(1-\varphi)(2+\varphi)}{3(2-\varphi)}, \quad (10)$$

$$k = \left( \frac{1}{(1-s)^2} - 1 \right) - \frac{4}{3} \frac{(1-\varphi)^3}{\varphi^2(2-\varphi)^2}. \quad (11)$$

186 Substitution of these two relations in Eq. 9 gives an implicit relation for the filtered  
187 fraction as a function of the solidity. Finally, because  $k$  is the coefficient for the pressure  
188 drop across one layer of the collector, the total pressure drop across multiple layers is obtained  
189 by multiplying  $k$  by the number of layers in the collector. The additivity of the pressure drop  
190 coefficient was confirmed by Eckert and Pflüger<sup>40</sup> when the distance between the screens is  
191 sufficient large. Idel’Cik estimates that the pressure drop across multiple layers is additive as  
192 long as the distance of separation between the layers exceeds 15 times the size of the threads  
193 (Idel’Cik,<sup>41</sup> page 291).

### 194 3 Results and discussion

195 To maximize the overall collection efficiency, we must seek a high filtered fraction ( $\varphi$ ) and  
196 a high incident fraction ( $\chi$ ). However, these quantities are maximized at opposite ranges of  
197 the parameters  $s$  and  $N$  (Figs. 2A,B). The results obtained in the previous section allow us  
198 to calculate the maximum ACE found at some intermediate values of these parameters.

199 As can be noted in Fig. 2B, the incident fraction  $\chi$  depends very nonlinearly on  $N$  which,  
200 at a glance, establishes the notable advantage offered by multi-layer designs. In a single-  
201 layer collector, the incident fraction cannot be maximized to unity, as this would imply  
202 complete obstruction of the mesh and thus no airflow through the collector. The use of  
203 several layers decouples, at least partially, the fluid mechanical processes behind the filtered  
204 fraction and the incident fraction. It is therefore possible to design the collector such that  
205 nearly all upstream droplets are on a collision course with one of the collector elements while

206 maintaining the solidity significantly below unity (Fig. 2B). Even for a relatively modest 5-  
207 layer collector, a solidity as low as 0.5 can already guarantee a near maximal incident fraction  
208 (Fig. 2B). The possibility of greatly increasing the incident fraction for intermediate solidity  
209 values is the reason why multi-layer collectors can be made much more efficient. Moreover,  
210 since the equation for the incident fraction is purely geometrical, there is no doubt about  
211 the general validity of this conclusion.

212 Computation of the aerodynamic collection efficiency  $\eta_{ACE} = \varphi\chi$  for a broad parameter  
213 range indicates that it reaches a maximum of 49% for  $N = 10$  (Fig. 2C). In contrast, single-  
214 layer collectors are confined to the line  $N = 1$  and can reach a maximal ACE of only 30% at  
215 an operational solidity slightly above 0.5. Increasing the number of layers beyond 10 increases  
216 the ACE further; with the theoretical possibility of reaching an ACE of unity for very large  
217  $N$  (Fig. 2D). This limiting behavior raises the question of how many layers should be used in  
218 practice. An answer emerges when considering the contribution to the total ACE made by  
219 each new layer (Fig. 2D). Beyond  $N = 5$ , the relative increase in ACE becomes vanishingly  
220 small. Therefore, considerations about the most efficient use of available materials would  
221 suggest that the number of layers should be limited to approximately 5, at least in the limit  
222 where  $d_\infty \rightarrow d$ .

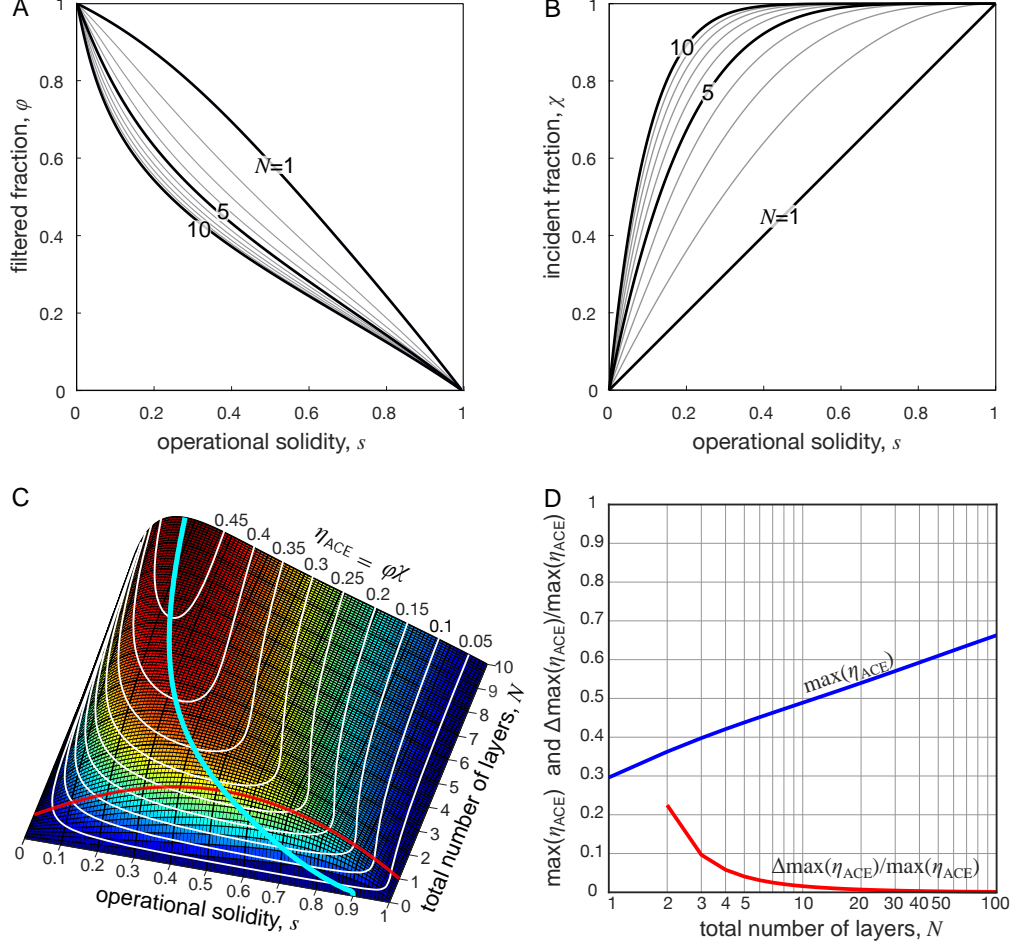


Figure 2: Aerodynamic collection efficiency for multi-layer fog collectors. (A) Filtered fraction predicted from the Steiros2018 model (Eqs. 9-11). (B) The incident fraction computed from geometrical considerations (Eq. 5, second term on the RHS). (C) The ACE Ridge - a 3D representation of ACE as a function of the two control parameters  $s$  and  $N$ . A maximum ACE of 0.49 is observed for 10 layers, each with an operating solidity of 0.17. The blue curve marks the subspace where  $\eta_{ACE}$  is maximized at constant  $N$ . Single-layer collectors are confined to the line  $N = 1$  and have an ACE below 0.3. (Note: we have treated  $N$  as a continuous variable for the purposes of illustration). (D) The maximal ACE as a function of  $N$  (plotted on a log scale). Although  $\max(\eta_{ACE})$  increases with increasing  $N$ , the relative ACE increase,  $\Delta\max(\eta_{ACE})/\max(\eta_{ACE})$ , becomes small for  $N > 5$  and negligible for  $N > 10$ .

223 As indicated in the theory section, the Steiros2018 model is one of many models, pub-  
 224 lished over a period of 80 years, that provide a fluid mechanical formulation for the filtered  
 225 fraction (Suppl. Mat). The functional form as well as the asymptotic behavior of the filtered  
 226 fraction predicted by alternative theories vary substantially (Fig. 3A). In that respect, the

227 Glauert1932 model<sup>42</sup> and the Rivera2011 model<sup>19</sup> represent two extreme behaviors, while  
 228 the Steiros2018 model<sup>39</sup> adopted here and its precursor, the Koo1973 model,<sup>38</sup> are interme-  
 229 diate for the limiting behavior of  $\varphi$  as  $s \rightarrow 0$ . The prediction of the models for small solidity  
 230 is especially important in the context of multi-layer collectors since their maximal ACE is  
 231 attained for solid fractions below 0.3 (Fig. 3B).

232 A comparative analysis of the design space for these models is also informative. Notably,  
 233 although the models disagree on the maximum  $\eta_{ACE}$  that can be achieved for a given  $N$ ,  
 234 their respective ACE ridges follow similar arcs in design space (Fig. 3B). Specifically, they all  
 235 go through a small target area ( $0.25 < s < 0.35$ ,  $N = 4, 5$ ) where the multi-layer collectors  
 236 achieve an efficiency  $\sim 40\%$  better than the most efficient single-layer collectors. The quanti-  
 237 tative agreement between the models shows the robustness of the efficiency optimization in  
 238 design space (see also Regalado and Ritter<sup>28</sup> for qualitatively similar results). Interestingly,  
 239 the subspace where  $\eta_{ACE}$  is locally maximized follows closely curves of constant filtered frac-  
 240 tion for all four models (Fig. S1). Therefore, the improved aerodynamic collection efficiency  
 241 of multi-layer fog collectors comes almost exclusively from improvements in the incident  
 242 fraction as new layers are added to the system.

243 Because the models differ substantially in their predicted maximum ACE (from 34% to  
 244 63% for a 10-layer collector), we undertook a series of observations to quantify the efficiency  
 245 on multi-layer collectors. As noted above, the equation for  $\eta_{ACE}$  is, first and foremost, a  
 246 statement about two geometrical ratios: the area ratio associated with the filtered fraction  
 247 and the solidity  $s$  of the mesh (ratio of obstructed area over the total area of one collector  
 248 layer). To assess the ACE, we developed a wind tunnel to produce realistic fog conditions  
 249 in the laboratory (Fig. 4A, Suppl. movie). Experimenting with a 4-layer harp collector  
 250 ( $l = 100$  mm,  $h = 2$  mm,  $d = 0.150$  mm), we found an operating solidity of  $s = 0.17$   
 251 (Figs. 4B,C), giving an incident fraction of  $\chi = 1 - (1 - s)^4 = 0.53$ . Integrating the flow  
 252 field, we arrived at a filtered fraction of  $\varphi_{obs} = (l_{\infty}/l)^2 = 0.81 \pm 0.016$  (Figs. 4D,E). Based  
 253 on the measured incident and filtered fractions, the aerodynamics collection efficiency is

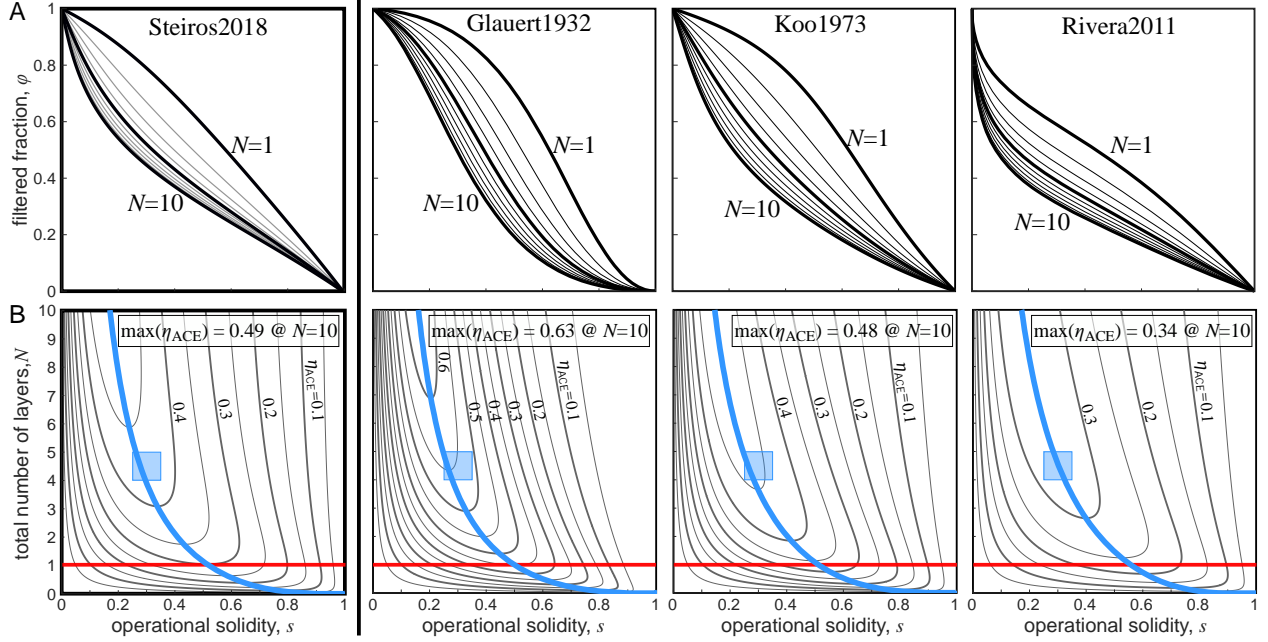


Figure 3: Comparative analysis of the ACE ridge. (A) The filtered fraction predicted by four fluid mechanics models. Note the model-dependent form of the asymptotic behavior of  $\varphi(s)$  as  $s \rightarrow 0$ . (B) Design space for the models listed in (A). The blue curve marks the subspace within which ACE is locally maximized at constant  $N$ . The blue square is the suggested target design. The red line at  $N = 1$  is the design space for single-layer collectors.

254  $\eta_{ACE} = \varphi\chi = 43\%$ , which exceeds slightly the value of 37% predicted by the Steiros2018  
 255 model (Fig. 2C). The discrepancy arises in part because of the impossibility of measuring the  
 256 flow field within 10 mm of the collector's surface with our current experimental set-up. The  
 257 truncated velocity field leads to an artificially inflated filtered fraction (Table S1, Fig. S2).  
 258 A better reconstruction of the velocity field could be achieved with other flow visualization  
 259 methods such as the smoke-wire technique.<sup>43</sup>

260 Given the care needed to measure ACE, it might be asked why it should be preferred as  
 261 a performance standard over the total water collection efficiency,  $\eta_{tot}$ , as defined in Eq. 1.  
 262 Although Eq. 1 appears trackable at first sight, a more detailed analysis (Eq. 3) reveals that  
 263  $\eta_{tot}$  involves the lost mass fraction,  $\int_0^\infty \left(1 - \frac{d_\infty(r)}{d}s\right)^N m(r)dr$ , where the terms  $\frac{d_\infty(r)}{d}$  and  
 264  $m(r)$  both depend on the radius of the droplets in the incoming fog. Notably, these two  
 265 terms give, together, a scaling on the order of  $r^5$  (see the Theory section). Therefore, unless  
 266 the probability density function for the droplet sizes,  $f(r)$ , is characterized precisely, the

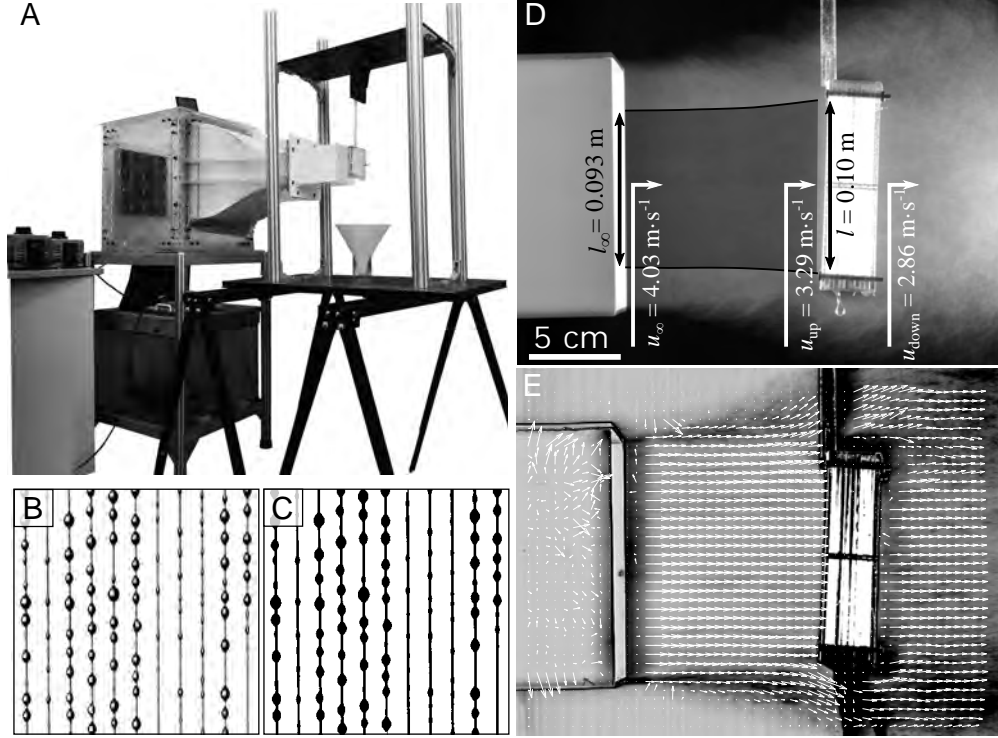


Figure 4: Measurement of ACE for a multi-layer harp collector ( $s = 0.17$ ,  $N = 4$ ). (A) Fog tunnel with  $14 \text{ cm} \times 14 \text{ cm}$  working section. (B) Photo of the mesh under operating conditions. (C) Binary (black/white) version of (B) used to compute the solidity. The “dry” solidity is 0.075 while the “wet”, operational solidity is 0.17. (D) Close-up of the fog jet filtering through the collector with the key variables characterizing the flow field indicated. (E) Detailed flow field used to infer the variables in (D). (see Suppl. Mat. for movie)

267 total water collection efficiencies are impossible to compare. In fact, it could be argued that  
 268 the very nonlinear dependence on  $r$  makes  $\eta_{tot}$  virtually useless as a metric for efficiency  
 269 because of its great sensitivity to the presence of rare but large droplets. ACE, in contrast,  
 270 is what is left of  $\eta_{tot}$  when factors affected by the droplet size structure of fog are eliminated  
 271 (Eq. 5). Moreover, ACE captures the fundamental trade-off for fog collection. Therefore, in  
 272 an effort to increase the repeatability and portability of future research in fog collection, we  
 273 propose the geometrical measurement of ACE as a potential standard for the field (Fig. S3).

274 As a final validation of the performance of multi-layer collectors, we compare their yield  
 275 with that of the standard fog collecting medium - two plies of Raschel mesh (“dry” solidity  
 276  $s = 0.6$ )<sup>44</sup> without spacing between them and thus approximating a single-layer collector. As  
 277 expected, the yield of the multi-layer harps greatly exceeded that of the Raschel standard

278 (Fig. 5). Notably, even a single harp layer offered a slightly better yield than the two-  
 279 ply Raschel mesh (Fig. 5B). The poor performance of the Raschel mesh under well-defined  
 280 laboratory conditions is explained by the fact that the two-ply mesh exceeds greatly the  
 281 optimal operational solidity ( $s_{Raschel} \simeq 0.7$  vs  $s_{opt} \simeq 0.5$ ). While the multi-harp designs  
 282 outperformed single-layer designs for all  $N$ , these collectors lose some of their yield for  
 283  $N \geq 6$  (Fig. 5B). This result is unlike what might be predicted from the design space. This  
 284 efficiency loss probably arises because of the increasing boundary layer that develops in the  
 285 vicinity of the collector frame. In the case of a 10-layer collector, the frame depth exceeds 50  
 286 mm while the open area for filtration remains  $100 \text{ mm} \times 100 \text{ mm}$ . In other words, for large  
 287  $N$ , the collector depth is such that the collector forms an increasingly long tube through  
 288 which the fog stream must flow. Despite this limitation, the five-layer harp offered a four-  
 289 fold increase in yield (Fig. 5B). These results were confirmed in field experiments with the  
 290 4-layer harp prototype shown in Fig. 1D. During a period of low fog, the prototype collected  
 291  $4.3 \text{ l}\cdot\text{day}^{-1}\cdot\text{m}^{-2}$  while the two-ply Raschel mesh collected only  $1 \text{ l}\cdot\text{day}^{-1}\cdot\text{m}^{-2}$  (Fig. 5C).

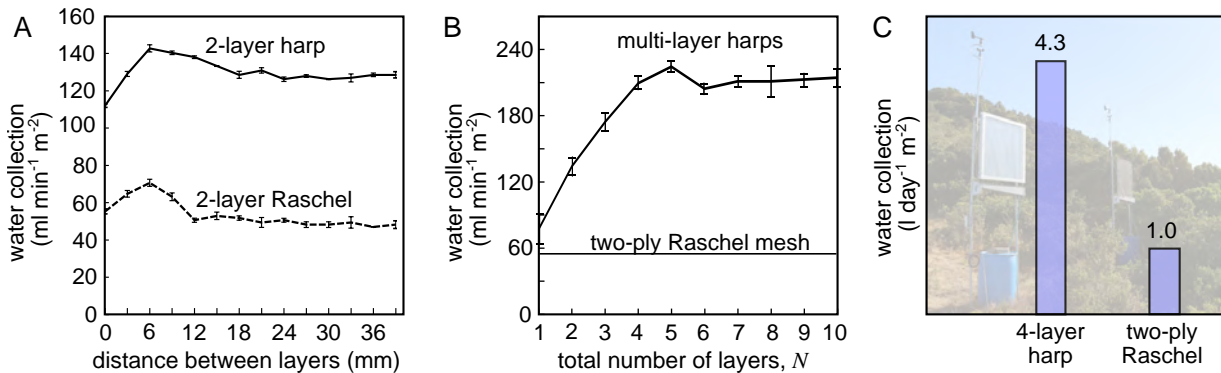


Figure 5: Yield measurements. (A) Effect of inter-layer spacing on the yield of multi-layer collectors. (B) Yield of multi-layer harps ( $1 \leq N \leq 10$ ,  $s = 0.17$ , inter-layer spacing of 6 mm) compared to two plies of Raschel mesh with  $s = 0.7$  at a fog velocity  $u_\infty = 4 \text{ m}\cdot\text{s}^{-1}$ . (C) Field measurements of yield over 20 days.

## 292 4 Conclusions

293 In this paper, we have presented designs for optimally efficient passive fog collectors by  
294 focusing on a geometrical relation (Eq. 5) known as the aerodynamic collection efficiency  
295 (ACE). As we have shown, the maximal values of ACE are achieved only through the use  
296 of multi-layer collectors whose efficiency can exceed by 40% that of the best single-layer  
297 collectors. The analysis shows that, taking into account the most effective use of materials,  
298 the optimal fog collector has  $N = 4, 5$  layers and operating solidity  $s = 0.3 \pm 0.05$ , assuming  
299 that the *operating* thread diameter is sufficiently small to maximize inertial impaction of fog  
300 droplets. These conclusions were validated experimentally for multi-layer harp collectors.  
301 When optimized, the latter can collect as much as four times that collected by the standard  
302 two-ply Raschel mesh, both under laboratory and field conditions.

## 303 5 Experimental

304 **Collector design** - Multi-layer collectors were built using fast prototyping tools. Using a  
305 laser cutter (Ready Cut), square plexiglass frames with a  $100 \text{ mm} \times 100 \text{ mm}$  central open  
306 area were fabricated. Evenly spaced notches (typical spacing:  $1 \text{ mm} \leq h \leq 2 \text{ mm}$ ) were  
307 made in the upper and lower edges of the frame to hold polyethylene monofilaments ( $d =$   
308  $150\text{-}160 \mu\text{m}$ ) into a vertical harp arrangement. These frames were then stacked with different  
309 inter-layer spacings to form multi-layer fog collectors.

310 **Yield measurements** - To measure the yield, the prototypes were hung at a distance of  
311  $100 \text{ mm}$  from the opening of a wind tunnel equipped with a fog chamber (see below). The  
312 water was collected in a funnel leading to a graduated cylinder. Collection occurred over a  
313 total time interval of  $15 \text{ min}$  following an initial saturation period of  $5 \text{ min}$ .

314 **Measurement of the aerodynamic collection efficiency** - Flow experiments were per-  
315 formed with an open-jet wind tunnel developed specifically to measure the efficiency of fog  
316 collector prototypes under natural conditions. The tunnel consists of two elements: a lower

317 nebulization chamber for fog production and an upper flow chamber to accelerate the fog  
318 cloud and guide it into a uniform jet (Fig. 4A). The nebulization chamber contained  $\sim 50$   
319 liters of water within which was immersed a 300 W 12-head ultrasonic nebulizer (Model  
320 DK12-36). The fog produced in this chamber was injected into the upper chamber using a  
321 16 W, 200 mm  $\times$  200 mm ventilation fan. Within the flow chamber, an array of 16, 80 mm  
322  $\times$  80 mm, computer fans accelerated the fog towards a contraction that converged the fog  
323 stream to a jet of 140 mm  $\times$  140 mm in cross-section. Both the ventilation fan and the array  
324 of computer fans were powered through variable voltage transformers allowing us to set the  
325 jet velocity in the range 0.1 – 4.2 m·s<sup>-1</sup>. A honeycomb filter was placed at the upstream end  
326 of the contraction to eliminate turbulence and provide a homogeneous fog flow.

327 The flow of fog through and around the collector prototypes was visualized using a  
328 Phantom V611 high speed camera equipped with a Canon EF 100 – 400mm telephoto  
329 zoom. Images were acquired at a rate of 4000 fps (exp. 240  $\mu$ s) with a camera resolu-  
330 tion of 1024  $\times$  768 pixels and an image scale of 270 $\mu$ m/pixel. Analysis of the flow pat-  
331 tern was performed using a Matlab program first developed by Dr. A.F. Forughi at the  
332 University of British Columbia (Vancouver, Canada) and made freely available on Github  
333 (<https://github.com/forughi/PIV>).

## 334 **Acknowledgement**

335 MA thanks the Technical University of Liberec (TUL) for a Student Grant (SGS 21313)  
336 2019. JD acknowledges funding from Fondef (ID15i10387) and Fondecyt (1130129). REG  
337 and AIP thank the Engineering and Physical Sciences Research Council (UK) for support  
338 under grant EP/M017982/.

## 339 **Supporting Information Available**

340 The following files are available free of charge.

- 341 • Supplementary Material: Table S1, Figures S1-S3, description of alternative fluid me-  
342 chanics models for the filtered fraction.
- 343 • Harp movie: movie of the fog flow through a 4-layer harp collector.

## 344 References

- 345 (1) *Sustainable Development Goal 6. Synthesis Report on Water and Sanitation*; United  
346 Nations: New York, 2018.
- 347 (2) Domen, J. K.; Stringfellow, W. T.; Camarillo, M. K.; Gulati, S. Fog water as an alter-  
348 native and sustainable water resource. *Clean Technologies and Environmental Policy*  
349 **2014**, *16*, 235–249.
- 350 (3) Schunk, C.; Trautwein, P.; Hruschka, H.; Frost, E.; Dodson, L.; Derhem, A.; Bargach, J.;  
351 Menzel, A. Testing water yield, efficiency of different meshes and water quality with a  
352 novel fog collector for high wind speeds. *Aerosol and Air Quality Research* **2018**, *18*,  
353 240–253.
- 354 (4) Beysens, D. *Dew Water*; River Publishers, 2018.
- 355 (5) Kaseke, K. F.; Wang, L. Fog and dew as potable water resources: Maximizing harvesting  
356 potential and water quality concerns. *GeoHealth* **2018**, *2*, 327–332.
- 357 (6) Gerasopoulos, K.; Luedeman, W. L.; Ölçeroglu, E.; McCarthy, M.; Benkoski, J. J. Ef-  
358 fects of engineered wettability on the efficiency of dew collection. *ACS Applied Materials*  
359 *& Interfaces* **2018**, *10*, 4066–4076.
- 360 (7) Kim, H.; Yang, S.; Rao, S. R.; Narayanan, S.; Kapustin, E. A.; Furukawa, H.;  
361 Umans, A. S.; Yaghi, O. M.; Wang, E. N. Water harvesting from air with metal-organic  
362 frameworks powered by natural sunlight. *Science* **2017**, *356*, 430–434.

- 363 (8) Schemenauer, R. S.; Cereceda, P. Fog-water collection in arid coastal locations. *Ambio*  
364 **1991**, *20*, 303–308.
- 365 (9) Schemenauer, R. S.; Cereceda, P. Fog collection’s role in water planning for developing  
366 countries. *Natural Resources Forum*. 1994; pp 91–100.
- 367 (10) Klemm, O. et al. Fog as a fresh-water resource: overview and perspectives. *Ambio*  
368 **2012**, *41*, 221–234.
- 369 (11) Park, K.-C.; Chhatre, S. S.; Srinivasan, S.; Cohen, R. E.; McKinley, G. H. Optimal  
370 design of permeable fiber network structures for fog harvesting. *Langmuir* **2013**, *29*,  
371 13269–13277.
- 372 (12) Cruzat, D.; Jerez-Hanckes, C. Electrostatic fog water collection. *Journal of Electrostat-*  
373 *ics* **2018**, *96*, 128–133.
- 374 (13) Damak, M.; Varanasi, K. K. Electrostatically driven fog collection using space charge  
375 injection. *Science Advances* **2018**, *4*, eaao5323.
- 376 (14) Holmes, R.; Rivera, J. D.; de la Jara, E. Large fog collectors: New strategies for collec-  
377 tion efficiency and structural response to wind pressure. *Atmospheric Research* **2015**,  
378 *151*, 236–249.
- 379 (15) Jiang, Y.; Savarirayan, S.; Yao, Y.; Park, K.-C. Fog collection on a superhydrophilic  
380 wire. *Applied Physics Letters* **2019**, *114*, 083701.
- 381 (16) Rajaram, M.; Heng, X.; Oza, M.; Luo, C. Enhancement of fog-collection efficiency of a  
382 Raschel mesh using surface coatings and local geometric changes. *Colloids and Surfaces*  
383 *A: Physicochemical and Engineering Aspects* **2016**, *508*, 218–229.
- 384 (17) Shi, W.; Anderson, M. J.; Tulkoff, J. B.; Kennedy, B. S.; Boreyko, J. B. Fog harvesting  
385 with harps. *ACS Applied Materials & Interfaces* **2018**, *10*, 11979–11986.

- 386 (18) Zhang, L.; Wu, J.; Hedhili, M. N.; Yang, X.; Wang, P. Inkjet printing for direct mi-  
387 cropatterning of a superhydrophobic surface: toward biomimetic fog harvesting sur-  
388 faces. *Journal of Materials Chemistry A* **2015**, *3*, 2844–2852.
- 389 (19) Rivera, J. D. Aerodynamic collection efficiency of fog water collectors. *Atmospheric*  
390 *Research* **2011**, *102*, 335–342.
- 391 (20) Labbé, R.; Duprat, C. Capturing aerosol droplets with fibers. *Soft Matter* **2019**,
- 392 (21) Andrews, H.; Eccles, E.; Schofield, W.; Badyal, J. Three-dimensional hierarchical struc-  
393 tures for fog harvesting. *Langmuir* **2011**, *27*, 3798–3802.
- 394 (22) Lin, J.; Tan, X.; Shi, T.; Tang, Z.; Liao, G. Leaf Vein-Inspired Hierarchical Wedge-  
395 Shaped Tracks on Flexible Substrate for Enhanced Directional Water Collection. *ACS*  
396 *Applied Materials & Interfaces* **2018**, *10*, 44815–44824.
- 397 (23) Azad, M.; Ellerbrok, D.; Barthlott, W.; Koch, K. Fog collecting biomimetic surfaces:  
398 Influence of microstructure and wettability. *Bioinspiration & Biomimetics* **2015**, *10*,  
399 016004.
- 400 (24) Jing, X.; Guo, Z. Durable lubricant-impregnated surfaces for water collection under  
401 extremely severe working conditions. *ACS Applied Materials & Interfaces* **2019**,
- 402 (25) Li, C.; Liu, Y.; Gao, C.; Li, X.; Xing, Y.; Zheng, Y. Fog Harvesting of a bioinspired  
403 nanocone-decorated 3D fiber network. *ACS Applied Materials & Interfaces* **2019**, *11*,  
404 4507–4513.
- 405 (26) LeBoeuf, R.; de la Jara, E. Quantitative goals for large-scale fog collection projects  
406 as a sustainable freshwater resource in northern Chile. *Water international* **2014**, *39*,  
407 431–450.

- 408 (27) Gischler, C. *The missing link in a production chain. Vertical obstacles to catch Caman-*  
409 *chaca*; UNESCO Regional Office for Science and Technology for Latin America and the  
410 Caribbean -ROSTLAC, Montevideo, Uruguay., 1991.
- 411 (28) Regalado, C. M.; Ritter, A. The design of an optimal fog water collector: A theoretical  
412 analysis. *Atmospheric Research* **2016**, *178*, 45–54.
- 413 (29) Ito, A.; Garry, K. Pressure measurements around a two-dimensional gauze at incidence.  
414 *Journal of Fluids and Structures* **1998**, *12*, 171–181.
- 415 (30) Goodman, J. The collection of fog drip. *Water Resources Research* **1985**, *21*, 392–394.
- 416 (31) Schemenauer, R. S.; Joe, P. I. The collection efficiency of a massive fog collector. *At-*  
417 *mospheric Research* **1989**, *24*, 53–69.
- 418 (32) Goodman, J. The microstructure of California coastal fog and stratus. *Journal of Ap-*  
419 *plied Meteorology* **1977**, *16*, 1056–1067.
- 420 (33) Cooper, C. D.; Alley, F. C. *Air pollution control: A design approach*; Waveland Press,  
421 2011.
- 422 (34) Demoz, B.; Collett Jr, J.; Daube Jr, B. On the Caltech active strand cloudwater col-  
423 lectors. *Atmospheric Research* **1996**, *41*, 47–62.
- 424 (35) Langmuir, I.; Blodgett, K. Mathematical investigation of water droplet trajectories. *GE*  
425 *Res. Lab. Rep., No. RL 225* **1945**,
- 426 (36) Morgan, P. Fluid flow through screens of low solidity. *The Aeronautical Journal* **1962**,  
427 *66*, 54–56.
- 428 (37) Taylor, G.; Davies, R. The aerodynamics of porous sheets. *Aeronautical Research Coun-*  
429 *cil, Reports and Memoranda* **1944**, *2237*, 163–176.

- 430 (38) Koo, J.-K.; James, D. F. Fluid flow around and through a screen. *Journal of Fluid*  
431 *Mechanics* **1973**, *60*, 513–538.
- 432 (39) Steiros, K.; Hultmark, M. Drag on flat plates of arbitrary porosity. *Journal of Fluid*  
433 *Mechanics* **2018**, *853*.
- 434 (40) Eckert, B.; Pflüger, F. *Technical Memorandum No. 1003: The resistance coefficient of*  
435 *commercial round wire grids*; National Advisory Committee for Aeronautics: Washing-  
436 ton, 1942.
- 437 (41) Idel’Cik, I. E. *Memento des pertes de charge*; Collection de la Direction des Etudes et  
438 Recherches d’Electricité de France, Eyrolles: Paris, France, 1969.
- 439 (42) Glauert, H.; Hirst, D.; Hartshorn, A. *The induced flow through a partially choked pipe*  
440 *with axis along the wind stream*; HM Stationery Office, 1932.
- 441 (43) Batill, S. M.; Mueller, T. J. Visualization of transition in the flow over an airfoil using  
442 the smoke-wire technique. *AIAA journal* **1981**, *19*, 340–345.
- 443 (44) Schemenauer, R. S.; Cereceda, P. A proposed standard fog collector for use in high-  
444 elevation regions. *Journal of Applied Meteorology* **1994**, *33*, 1313–1322.

445 Graphical TOC Entry

446

